ADVANCES IN ATMOSPHERIC SCIENCES, VOL. 44, MARCH 2026, 1–14

• **Original Paper** •

Northward Shift of the Tibetan Plateau Vortex Street–like System Intensifies Mid- and Late-Summer Rainfall Extremes in Beijing

Ruyu GAN[1,2] and Gang HUANG[*2,3]

[1]*Ocean College, Jiangsu University of Science and Technology, Zhenjiang, China*

[2]*Key Laboratory of Earth System Numerical Modeling and Application, Institute of Atmospheric Physics, Chinese Academy of Sciences, Beijing, China*

[3]*University of Chinese Academy of Sciences, Beijing, China*

(Received 28 August 2025; revised 17 December 2025; accepted 7 January 2026)

ABSTRACT

During 24–28 July 2025, Beijing and its surrounding regions experienced a record-breaking rainfall event that triggered severe flooding, resulting in substantial economic losses and casualties. Here, we show that this extreme rainfall was strongly influenced by a vortex street–like system in the wake of the Tibetan Plateau (TPVSL), a large-scale dynamical feature that constitutes a key mechanism within the East Asian subtropical main rain belt. Using daily reanalysis data and precipitation observations, we demonstrate that the TPVSL provided the background circulation field for more than 90% of the rainfall during this event. The propagation line of the TPVSL exhibited an anomalous northward displacement in July 2025, closely linked to the abnormal northward position of the western Pacific subtropical high (WPSH). In contrast, the vortex propagation speed and shedding period of the TPVSL remained comparable to climatological conditions. We further show that the July 2025 northward shift of the WPSH is consistent with a long-term trend, as the WPSH has migrated northward by 1°–2° latitude during July–August from 1979 to 2024. This secular displacement has driven a concurrent northward shift of the TPVSL propagation line, resulting in increasing summer rainfall and heavy precipitation events in northern China, including the Beijing region. Our findings highlight the crucial role of the TPVSL system in shaping extreme rainfall in North China and provide a new perspective for understanding and mitigating flood risk in Beijing.

Key words: summer rainfall, Beijing, western Pacific subtropical high, Tibetan Plateau, vortex street–like system

Citation: Gan, R. Y. and G. Huang, 2026: Northward shift of the Tibetan Plateau vortex street-like system intensifies mid- and late-summer rainfall extremes in Beijing. *Adv. Atmos. Sci.*, **44**(1), 1−14, https://doi.org/10.1007/s00376-026-5565-z.

Article Highlights:

- 90% of Beijing's extreme rainfall occurred within the TPVSL structure during the event.
- Abnormal northward shifts of the WPSH and TPVSL in July 2025 positioned the rain belt over the Beijing region.
- Long-term northward movements of the TPVSL and WPSH increase Beijing's extreme precipitation probability.

1. Introduction

In late July 2025 (24–28 July), Beijing experienced a prolonged episode of extreme rainfall, the most intense event of the flood season that year. The average precipitation over Miyun District exceeded 300 mm, triggering severe flash floods, landslides, and widespread urban inundation. The disaster resulted in 44 fatalities and affected more than 300 000 people. As the political, economic, and cultural center of China, the city's highly concentrated population and infrastructure amplified the socioeconomic impacts far beyond those observed in ordinary regions. This event therefore drew broad attention from both society and the scientific community. Understanding its large-scale drivers and climatic background is essential for improving disaster prevention, mitigation, and adaptation strategies in the region.

The event occurred during the rainy season of North China, one of the three major monsoon rainy seasons in China. Under the prevailing East Asian summer monsoon, a rain belt typically establishes over North China in mid- to late July and persists for several weeks (Ding and Chan, 2005). Compared with the presummer rainy season over South China and the mei-yu season over the Yangtze–Huaihe River valley, the total precipitation during the North China rainy season is smaller. However, daily and even hourly precipitation extremes can reach comparable or higher intensities, frequently producing severe disasters (Luo et al., 2016). For instance, the record-breaking Beijing "7·21" storm in 2012 claimed 79 lives and caused nearly 2 bil-

* Corresponding author: Gang HUANG
Email: hg@mail.iap.ac.cn

lion USD in direct economic losses (Zhang et al., 2013; Zhou et al., 2013). The "75·8" rainfall in Henan in 1975 led to more than 26 000 fatalities and damages of about 1.5 billion USD (Ding, 2015). More recently, the "21·7" event in Henan in 2021 resulted in 398 deaths and 18 billion USD in economic losses (Fu et al., 2022a; Luo et al., 2023; Zhang et al., 2023). Zhang et al. (2023) reviewed recent studies and showed that the 2021 Henan record-breaking rainfall was associated with an anomalous, moisture-rich large-scale circulation and intensified by interacting mesoscale systems, while remaining difficult to predict because of complex multiscale dynamics.

Summer precipitation in northern China is closely tied to anomalies in the East Asian summer monsoon, with sea surface temperature variability, snow and sea-ice conditions, and large-scale circulation systems identified as key drivers (Huang and Wu, 1989). For extreme rainfall events in this region, previous studies have further emphasized the critical role of large-scale circulation in driving extreme summer rainfall over North China (Zhao et al., 2019b; Chen and Zhang, 2020; Xu et al., 2022). For example, Xu et al. (2022) showed that the 2021 "21·7" Henan flood occurred under an extreme dipole circulation, characterized by an anomalously northward and westward extended western Pacific subtropical high (WPSH), which sustained persistent southeasterly moisture transport and intense moisture flux convergence. Several prominent large-scale circulations, such as the WPSH, upper-level westerly jets, midlatitude baroclinic systems, and low-level vortices are closely tied to extreme precipitation over North China (Sun et al., 2015; Zhao et al., 2019a, 2019b). In particular, westward extension and northward displacement of the WPSH substantially alter East Asian monsoon circulations and moisture transport pathways, thereby influencing both the intensity and spatial distribution of heavy rainfall across North China (Orsolini et al., 2015; Zhao et al., 2019b). In addition, tropical cyclones (TCs) exert a strong influence on the position and intensity of the WPSH, which in turn regulates moisture transport toward eastern China during the warm season (Ding and Chan, 2005). Many case studies have documented that extreme rainfall over North China is often accompanied by TC activity over the western North Pacific, which facilitates the establishment and intensification of southeastward moisture channels (Chen et al., 2023).

Beyond these large-scale factors, mesoscale vortices also act as important triggers of extreme rainfall in North China. Previous studies have demonstrated that vortex activity substantially affects heavy rainfall over Southwest, East, and North China (Li et al., 2021; Fu et al., 2022b). Southwest vortices, for example, are important heavy rainfall–producing systems that can intensify and propagate northeastward, sometimes developing into Huang–Huai cyclones and exerting far-reaching influences on rainfall over North China (Tao and Ding, 1981; Fu et al., 2022a). Several severe rainfall events in Henan have been closely linked to the eastward migration of southwest vortices, underscoring their role as key precursors of heavy rainfall in northern China (Wang and Liu, 2017). Recent work has further revealed that extreme mei-yu seasons are often accompanied by more frequent and intense vortex activity; vortices repeatedly develop and persist under the combined influence of the WPSH and upper-level troughs and ridges, sustaining prolonged heavy rainfall (Fu et al., 2022a). Meanwhile, Tibetan Plateau vortices (TPVs) not only become critical precipitation-triggering systems after moving off the plateau but also influence eastern China through their lifecycle over the plateau by modulating large-scale circulation (Li et al., 2021). Collectively, these findings suggest that the coupling between large-scale systems (e.g., the WPSH, TCs, and troughs/ridges) and mesoscale features (e.g., vortices and shear lines) is fundamental to the occurrence and persistence of extreme rainfall over North China.

Early theoretical work proposed that the westerly flow around the Tibetan Plateau may generate quasi-periodic vortex streets on its eastern flank, akin to a Kármán vortex street, thereby modulating anomalous vortex activity in East Asia (Yeh and Gao, 1979; Ding, 1992; Wu, 1999). This concept of a "Tibetan Plateau vortex street" has even been incorporated into meteorological textbooks (Wu, 1999). More recently, Liu et al. (2023) quantitatively identified and diagnosed the Tibetan Plateau vortex street (hereafter TPVSL), showing that it provides favorable background conditions for more than 80% of precipitation over much of East Asia. They further demonstrated that the TPVSL acts as a major trigger of the subtropical rain belt and as an important source of precipitation variability on 3–7-day timescales (Liu et al., 2008, 2023, 2025). More recently, Liu et al. (2025) analyzed the extreme rainfall events of June–July 2020 and June–July 2024 and highlighted the critical role of the TPVSL in both cases. Together with the climatological evidence that the TPVSL provides a favorable background for 80%–90% of precipitation and heavy-rain days along the East Asian subtropical rain belt, including North China (Liu et al., 2023), these findings suggest that the TPVSL is a key dynamical ingredient of regional summer rainfall and extremes. This motivates us to investigate whether the TPVSL also provided an important background circulation for the extreme rainfall around Beijing in July 2025.

These considerations naturally raise two key questions: Was the July 2025 Beijing rainfall episode influenced by the effect of the TPVSL? And under global warming, have such extreme summer rainfall events over Beijing exhibited discernible long-term or interdecadal changes? To address these questions, this study aims to (1) evaluate the role of the TPVSL in the 24–28 July 2025 Beijing rainfall event, and (2) analyze the long-term spatiotemporal changes of summer extreme rainfall in Beijing and its surroundings, and their connections with the TPVSL and related circulation systems.

The remainder of this paper is organized as follows. Section 2 introduces the data and methods. Section 3 first examines the spatiotemporal correspondence between the TPVSL and the July 2025 Beijing rainfall and investigates the modulation of the TPVSL by the WPSH circulations. It then

presents the long-term evolution of summer rainfall and the roles of the TPVSL and associated circulation fields in these trends. Section 4 discusses the implications and concludes the study.

2. Methods

2.1. *Observational, reanalysis, and model data*

Daily precipitation data for 1 January 1979 to 15 August 2025 are obtained from the Climate Prediction Center (CPC) dataset, available at a 0.5° × 0.5° horizontal resolution (Chen et al., 2008). The daily and hourly mean horizontal wind, air temperature fields, convective available potential energy (CAPE), and moisture flux, on a 0.5° × 0.5° horizontal grid, from the fifth generation ECMWF atmospheric reanalysis (ERA5) (Hersbach et al., 2020) are used to characterize the associated circulation. The daily and six-hourly mean horizontal wind and air temperature fields on a 2.5° × 2.5° horizontal grid from the National Centers for Environmental Prediction–National Center for Atmospheric Research (NCEP/NCAR) reanalysis (Kalnay et al., 1996) are also used in this study. We note that the key findings in this study are not sensitive to the selection of the NCEP–NCAR or ERA5 dataset. These reanalysis datasets have been validated as effective for resolving mesoscale vortex activity (Curio et al., 2019). The stability of our results is confirmed across temporal scales, with consistent findings obtained from both daily and six-hourly analyses (Liu et al., 2023).

The WPSH is described by the 500-hPa eddy geopotential height, computed as deviations from the zonal mean between 0° and 40°N. The northern boundary of the WPSH is identified as the latitude where the 500-hPa eddy geopotential height first exceeds zero. The latitude of the upper-level westerly jet is determined from 200-hPa zonal winds following Kong and Chiang (2020), which are widely used as a reliable proxy for jet location. To examine the reanalysis-based findings, we additionally analyze historical model simulations from ACCESS-ESM1-5 within the CMIP6 archive (O'Neill et al., 2016). The model output spans the period from 1 January 1950 to 30 December 2014, providing an independent dataset to evaluate the reproducibility of key results. All model variables are interpolated onto a common 2.5° × 2.5° horizontal grid using bilinear interpolation prior to analysis.

2.2. *Identification of the TPVSL system and diagnostics*

The TPVSL system is identified from six-hourly and daily 700-hPa relative vorticity fields using a spatial Fourier transform—a technique commonly employed to extract large-scale wave structures (Wheeler and Kiladis, 1999). The vorticity field is decomposed into large-scale and small-scale components, with perturbations of meridional wavelengths shorter than 5° and zonal wavelengths shorter than 10° removed to suppress mesoscale variability. These thresholds are consistent with the intrinsic spatial scale of the TPVSL, whose width is typically 1000 km and whose vortex separation is approximately 2000 km in summer (Liu et al., 2023).

The resulting low-pass fields exhibit atmospheric counterparts of von Kármán vortex streets, with alternating rows of cyclonic and anticyclonic vortices of comparable scale (Liu et al., 2023). The TPVSL pathway is reconstructed by sequentially linking the centers of vortices detected in the lee-side region (Curio et al., 2019).

To comprehensively describe TPVSL behavior, we evaluate five diagnostics: (a) latitudinal position, determined from the temporal variation in the mean latitude of the reconstructed TPVSL pathway; (b) intensity, calculated as the mean positive 700-hPa filtered relative vorticity averaged over (35°–45°N, 105°–122.5°E); (c) propagation speed, estimated as the mean eastward translation velocity of the identified vortices; (d) shedding period, defined as the average time interval between the formation of successive vortices; (e) Strouhal number (S), used to characterize the standard oscillation of the flow and expressed as $S = T_e U_0/d$, where U_0 denotes the upstream wind speed, d represents the cross-wind scale of the Plateau at the dividing-streamline height (h_c), and T_e is the vortex shedding period.

2.3. *Quantification of TPVSL-related precipitation and heavy rainfall*

The TPVSL system plays an important role in modulating regional precipitation. To isolate its cyclonic contribution, we retained only positive vorticity anomalies by setting negative values in the low-pass filtered vorticity fields to zero. Precipitation influenced by TPVSL activity was identified following the outermost closed contour (OCC) approach, where the OCC corresponds to the zero line of the filtered relative vorticity (Hanley and Caballero, 2012). Within this boundary, precipitation coinciding with positive vorticity was regarded as TPVSL-related precipitation (Pr_TPVSL).

Heavy rainfall events were further characterized as days with daily totals exceeding 50 mm inside the OCC under positive vorticity conditions, which were aggregated to form a field of TPVSL-related heavy rainfall days (HRD_TPVSL). The proportional contributions of these components were quantified using the following ratios, reported in the text as percentages:

$$\text{Ratio1} = \frac{\text{Pr\_TPVSL}}{\text{Pr\_Total}}, \tag{1}$$

$$\text{Ratio2} = \frac{\text{HRD\_TPVSL}}{\text{HRD\_Total}}, \tag{2}$$

where Pr_Total denotes total precipitation during the study period. Analyses were conducted over a key domain of (35°–45°N, 105°–122.5°E).

2.4. *Vorticity budget diagnosis*

We diagnose the dynamical evolution of the TPVSL system using the pressure-coordinate vorticity budget following

the formulation of Holton (1992) and previous budget studies of mesoscale vortices (Kirk, 2003; Fu et al., 2017, 2025). The relative vorticity tendency at a given pressure level is written as follows:

$$\frac{\partial \zeta}{\partial t} = -\left(u\frac{\partial \zeta}{\partial x} + v\frac{\partial \zeta}{\partial y}\right) - \omega\frac{\partial \zeta}{\partial p} - (\zeta + f)(\nabla_h \cdot V_h) + \left(\frac{\partial u}{\partial p}\frac{\partial \omega}{\partial y} - \frac{\partial v}{\partial p}\frac{\partial \omega}{\partial x}\right) - \beta v + \mathrm{RES}\,. \quad (3)$$

Here, ζ is the relative vorticity; u and v are the horizontal winds, $\omega = \mathrm{d}p/\mathrm{d}t$ is the vertical velocity, and f is the Coriolis parameter. The terms on the right-hand side represent horizontal vorticity advection (HAV), vertical advection (VAV), stretching (STR), tilting (TIL) and the planetary vorticity advection (BETA). The residual term (RES) arises from friction, unresolved processes and numerical truncation. All terms are expressed in units of s^{-2}.

ERA5 hourly fields at a 1° × 1° resolution for July 2025 are used. The u, v and ω fields at standard pressure levels from 1000 to 300 hPa are extracted. After calculating each term at all pressure levels, the 700-hPa fields are extracted for analysis. To evaluate the role of the vortex during the rainfall peak, all vorticity budget terms are averaged over the Beijing region (39°–41°N, 116°–118°E) and over the period 1700 UTC 28 July to 0200 UTC 29 July 2025.

2.5. *Sensitivity experiment by removing the TPVSL from the model initial field*

Our sensitivity experiment utilized version 4.2 of the Advanced Research version of the Weather Research and Forecasting (WRF) model (ARW v4.2) to numerically simulate the extreme precipitation event in Beijing in late July 2025. The model was forced by the ERA5 data, with a horizontal resolution of 0.25° × 0.25°, providing the initial conditions and hourly lateral boundary conditions. The integration period was from 0000 UTC 23 July to 0000 UTC 26 July 2025, totaling 72 hours, covering the occurrence and development stages of the Beijing heavy rainfall.

The model employed a two-domain nested setup: the outer domain (D01) had a horizontal resolution of 20 km, covering most of China and key moisture source regions such as the northern Indian Ocean and the northwestern Pacific; the inner domain (D02) had a resolution of 4 km, focusing on Beijing and its surrounding areas. The number of vertical layers was 38.

Regarding physical parameterizations, the Kain–Fritsch cumulus scheme (Kain, 2004) was used for the outer domain. The WSM6 scheme (Hong and Lim, 2006) was employed for cloud microphysics; the RRTMG scheme (Iacono et al., 2008) for longwave and shortwave radiation; the Noah Land Surface Model for land surface processes (Chen and Dudhia, 2001); and the YSU scheme (Hong et al., 2006) for the planetary boundary layer.

To assess the impact of the TPVSL on this Beijing heavy rainfall event, we designed a sensitivity experiment to remove the TPVSL. The control experiment (CTRL) represents the original numerical simulation driven by the unmodified ERA5 initial and lateral boundary conditions. In the sensitivity experiment, NO_TPVSL, we quantitatively weakened the dynamic and thermodynamic perturbations associated with the TPVSL when constructing the ERA5 initial and lateral boundary conditions. The specific procedure is as follows.

First, the TPVSL vortex centers during 23–27 July 2025 were identified based on ERA5 700-hPa relative vorticity and wind fields, and a circular region of influence with a radius of approximately 800 km was defined around each center. Secondly, within the approximate TPVSL activity layer (about 950–600 hPa), the ERA5 horizontal wind, temperature, and specific humidity fields were decomposed into a large-scale background field (obtained through multiple passes of nine-point smoothing) and a residual perturbation field. The smoothing retained planetary-scale and large-scale background circulation while filtering out meso- and small-scale vortices. This method is widely used to analyze the elimination of the impact of cyclone activity on heavy rainfall (Davis and Low-Nam, 2001).

3. Results

3.1. *Contribution of vortex activity to heavy rainfall over Beijing and surrounding regions*

We first examine the daily evolution of the vorticity and circulation fields over 35°–50°N during 24–27 July 2025 (Figs. 1a–d). The spatially filtered relative vorticity fields (Figs. 1a–d) exhibit a striking resemblance to the canonical schematic of a vortex street (Fig. 1e), characterized by alternating bands of cyclonic and anticyclonic vortices downstream of the Tibetan Plateau. A train of positive vorticity anomalies, flanked by their negative counterparts, emerges in the lee region, consistent with the structural attributes of a TPVSL. These vortices coincide with the record-breaking rainfall over Beijing and surrounding areas, with the majority of precipitation occurring within cyclonic sectors of the vortex street. In addition, large-scale negative vorticity around 35°N to the southeast reflects the circulation of the WPSH, while two intense positive vorticity centers (20°–30°N) in the eastern domain correspond to the northward migration of Typhoons Francisco and Co-may. In the following sections, we demonstrate that these vortices satisfy the defining criteria of the TPVSL and quantify their substantial contribution to Beijing's rainfall, as well as their modulation by the WPSH.

The CPC dataset reveals the spatial structure of precipitation anomalies during the 24–29 July 2025 episode (Figs. 2a, b). Two dominant centers of positive anomalies are identified: one over the Beijing–Tianjin–Hebei metropolitan region and another across parts of Inner Mongolia and Shanxi Province. Both regions experienced cumulative rainfall anomalies exceeding 200 mm. The Beijing region is particularly critical given its exceptionally high population density and concentration of socioeconomic assets, amplifying

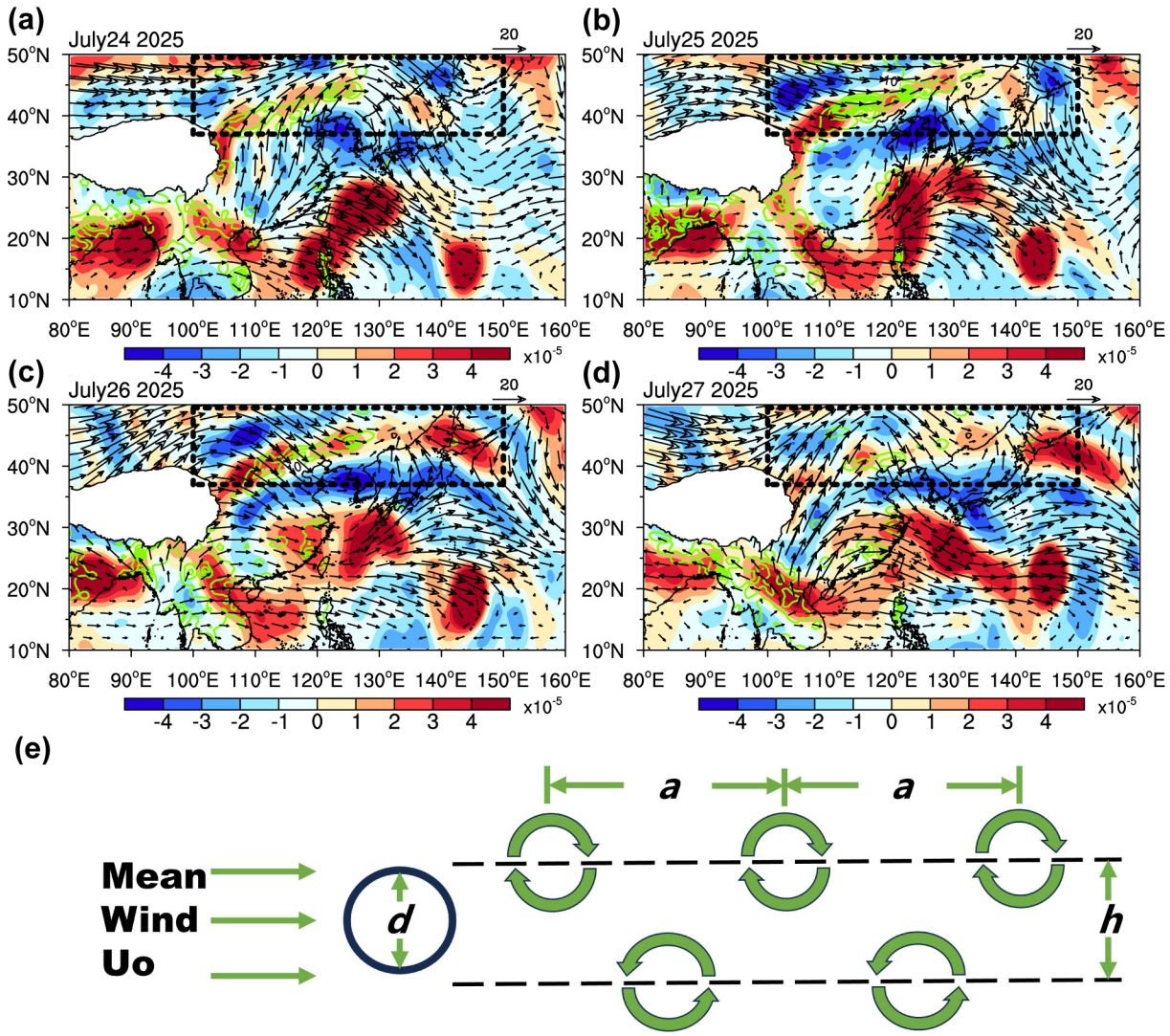

Fig. 1. Spatiotemporal structure of the TPVSL and associated precipitation during 24–27 July 2025. (a–d) Daily 700-hPa relative vorticity anomalies over 35°–50°N (black rectangle) after spatial low-pass filtering on (a) 24, (b) 25, (c) 26, and (d) 27 July 2025 (shading; units: 10^{-5} s^{-1}). The negative vorticity near 35°N represents the western Pacific anticyclone, while the two positive vorticity centers between 20°–30° correspond to Typhoons Francisco and Co-may. Green contours denote daily precipitation (interval: 10 mm). Both 700-hPa vorticity and 700-hPa wind vectors (units: m s^{-1}; vector scale in the lower right) are masked over the Tibetan Plateau for clarity of visualization (white shading). (e) Conceptual schematic of a Kármán vortex street generated by flow past a cylindrical obstacle, represented here by the Tibetan Plateau, in which *h* denotes the spacing between the cyclonic and anticyclonic rows of vortices, and *d* denotes the effective cross-stream diameter of the plateau. The observed configuration exhibits alternating anticyclonic vortices to the north and cyclonic vortices to the south, consistent with the wake dynamics induced by the westerly flow impinging on the plateau.

the disaster risk associated with this extreme event.

To further quantify the anomalies, we defined an analysis domain of the Beijing region of the Beijing metropolitan region. For 24–28 July 2025, the domain-mean precipitation reached 205 mm in the Beijing sector (Fig. 2c), accounting for approximately 40% of the local annual total. These values underscore the unprecedented intensity of this event within both a daily and monthly context.

The role of vortex activity was quantified by filtering the 700-hPa relative vorticity field to isolate TPVSL-related components and subsequently attributing precipitation to the cyclonic sectors of the system (see Methods). The results show that vortex activity accounted for most of the precipitation during the event (Figs. 2b, c). The rapid intensification of precipitation occurs simultaneously with the rapid enhancement of vortex street vorticity (Fig. 2d).

3.2. *Dynamical contribution of the TPVSL vortex to the Beijing extreme rainfall*

During late July 2025, the Beijing region experienced a rapid intensification of rainfall, with hourly precipitation rising sharply after 0000 UTC 26 July. To further assess whether the TPVSL vortex dynamically contributed to the Beijing extreme rainfall, we examined the time–pressure evo-

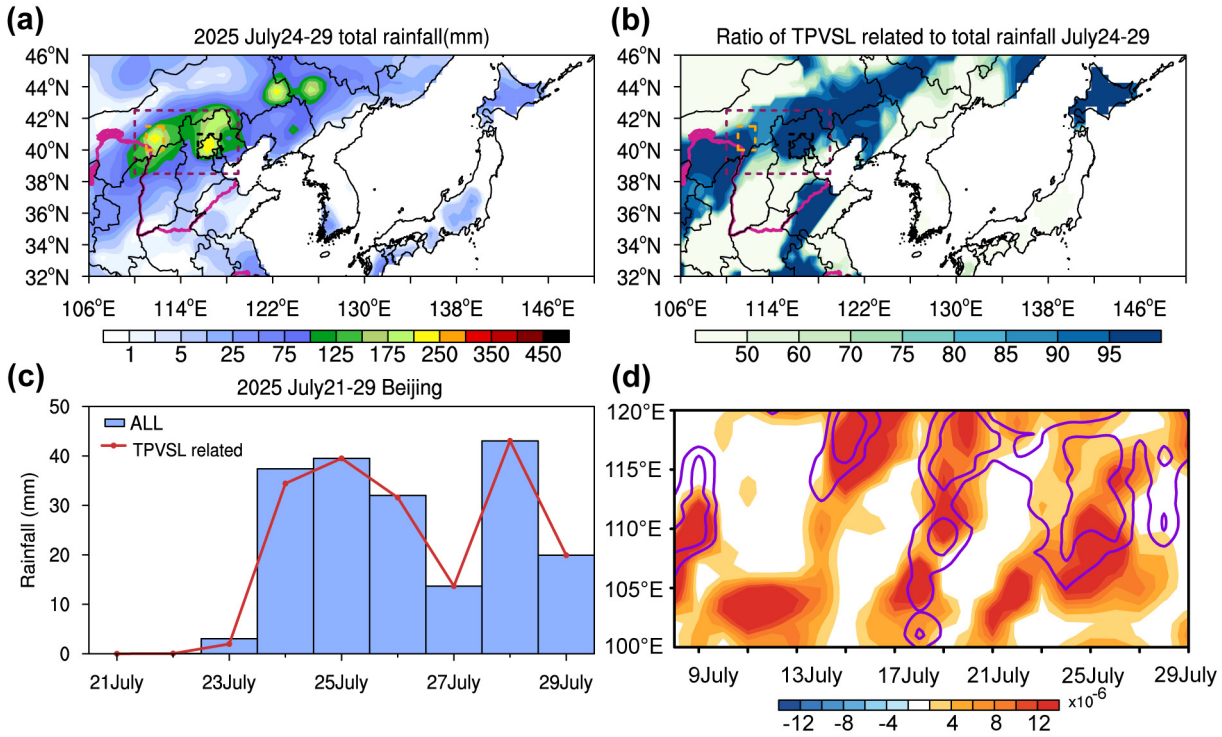

Fig. 2. Contribution of TPVSL activity to precipitation during 24–27 July 2025. (a) Spatial distribution of precipitation associated with cyclonic vortices embedded in the TPVSL during 24–27 July 2025. The purple, black, and orange rectangles denote the domains used to define North China, the Beijing region, and Inner Mongolia, respectively. (b) Fraction of precipitation linked to TPVSL cyclonic activity relative to the total precipitation during the same period (%, shading). (c) Time series of daily precipitation (bars) and the fraction attributable to TPVSL activity (red line) averaged over the Beijing region from 21–30 July 2025. (d) Hovmöller diagram of low-pass filtered daily 700-hPa relative vorticity averaged over 35°–45°N during 8–29 July 2025 (shading; units: 10^{-6} s^{-1}), with overlaid daily mean precipitation along the same latitudinal band (purple contours at 10 and 20 mm d^{-1}).

lution of the vorticity budget averaged over the Beijing region (Fig. 3). From 26 to 29 July, a sustained positive vorticity tendency is evident throughout the mid-troposphere, with the strongest signal concentrated between 850 and 600 hPa during the rainfall peak.

Horizontal advection provides a sustained positive contribution before and during the rainfall peak, indicating a continuous import of cyclonic vorticity associated with the eastward-propagating TPVSL system. During the peak rainfall period, the stretching term becomes increasingly important over Beijing, consistent with enhanced low-level convergence and column stretching linked to deep convection. Vertical advection and tilting remain comparatively weak and contribute little to the net tendency. Similar vorticity budget behavior has been reported for long-lived convective vortices associated with extreme hourly precipitation (Fu et al., 2022b).

Together, these diagnostics demonstrate that the TPVSL system did not simply coincide with the rainfall in time and space but dynamically intensified over Beijing during the peak rainfall period. The dominant stretching contribution, supported by horizontal transport of cyclonic vorticity, provides strong physical evidence that the vortex system played an active and important role in organizing the extreme precipitation.

3.2. *A series of vortices exhibit the characteristics of a TPVSL system*

A key question is whether the extreme precipitation observed during the late July 2025 Beijing event was linked to the TPVSL system. The circulation fields exhibit strong resemblance to the TPVSL pattern, characterized by alternating cyclonic and anticyclonic vortices between 35°N and 45°N (Figs. 1a–d). The meridional spacing of the vortex pairs closely matches the north–south extent of the Tibetan Plateau, consistent with the geometric constraints of vortex street dynamics. Figure 2a compares the idealized TPVSL structure with the observed spatiotemporal patterns of 700-hPa relative vorticity and precipitation during 24–28 July 2025. Positive vorticity centers emerged at quasi-regular intervals of 4–6 days and propagated eastward into the Pacific. These features closely resemble the Kármán vortex-street patterns reported in laboratory experiments (Chopra and Hubert, 1965) and documented within the subtropical East Asian rainbelt (Liu et al., 2023). The temporal evolution of precipitation anomalies aligns closely with the propagation of these vortices, providing additional evidence for the influence of the TPVSL.

Based on the north–south extent of the Tibetan Plateau (~1000 km) and the typical July 700-hPa upstream velocity of 10 m s^{-1}, the vortex shedding period is estimated at

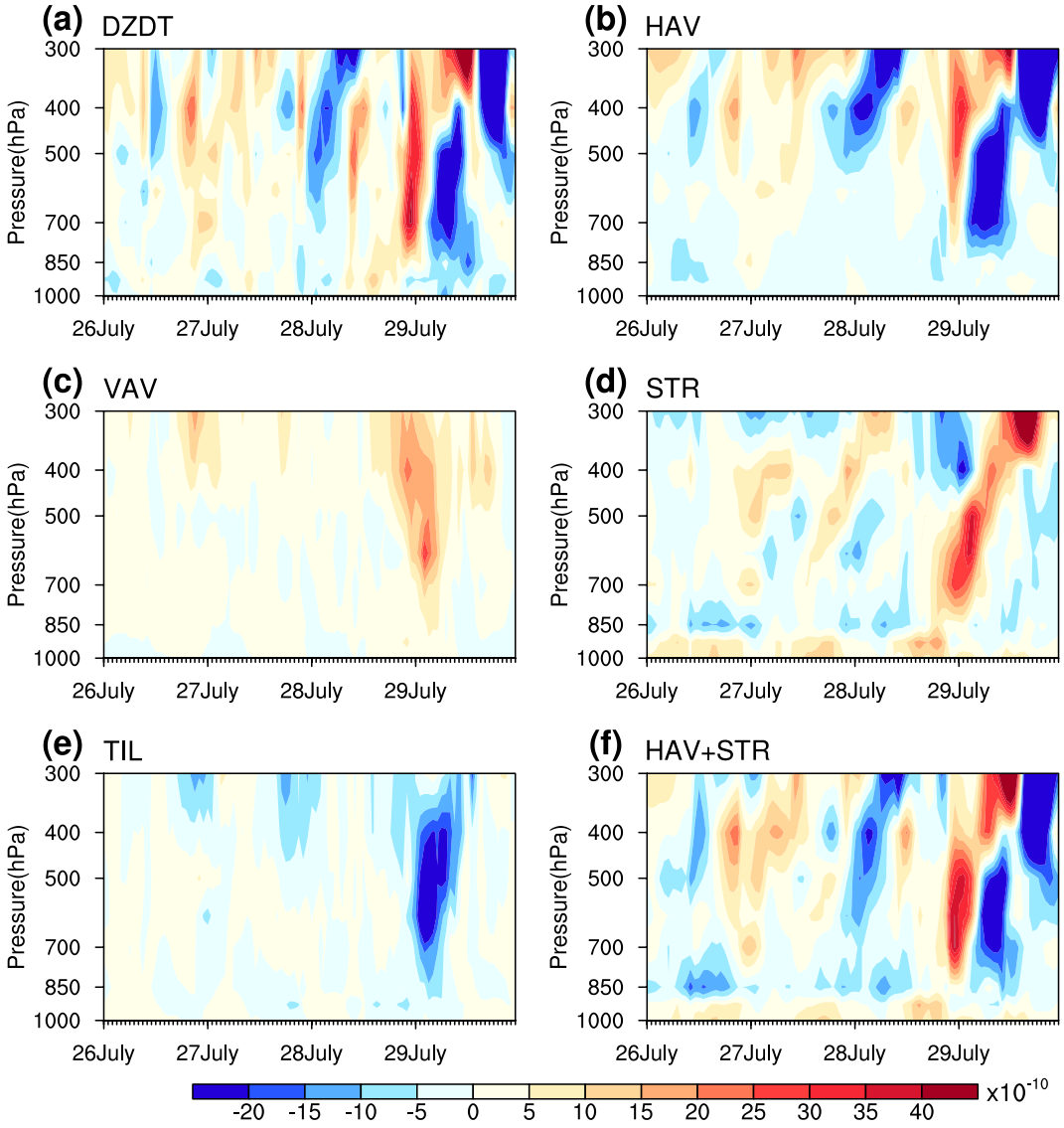

Fig. 3. Time–pressure evolution of the vorticity budget associated with the TPVSL vortex during the Beijing extreme rainfall event. Time–pressure cross sections of area - mean vorticity budget terms averaged over the Beijing region (38°–41°N, 115°–118°E) from 0000 UTC 26 July to 0000 UTC 29 July 2025: (a) local vorticity tendency (DZDT, 10^{10} s^{-2}); (b) horizontal vorticity advection (HAV, 10^{10} s^{-2}); (c) vertical vorticity advection (VAV, 10^{10} s^{-2}); (d) stretching term (STR, 10^{10} s^{-2}); (e) tilting term (TIL, 10^{10} s^{-2}); (f) combined contribution of horizontal advection and stretching (HAV + STR, 10^{10} s^{-2}). Positive values indicate cyclonic vorticity amplification.

roughly five days. This value corresponds to a Strouhal number near 0.2, consistent with the theoretical expectation for vortex shedding (Bearman, 1967). The estimated shedding period aligns well with observational diagnostics reported in previous studies (Liu et al., 2023). The Reynolds number for the flow around the Tibetan Plateau is approximately 10 000 (Liu et al., 2023), satisfying the condition for the existence of a Kármán vortex street (50–10^{+5}). The spatial distribution of the TPVSL closely resembles that of fluid dynamics simulation experiments of a Kármán vortex street with a Reynolds number of 10 000 (Khan et al., 2017). Taken together, the evidence suggests that the wake of the Tibetan Plateau in July 2025 developed into a well-defined vortex street–like system, with the most intense rainfall over Beijing and nearby areas occurring under its influence. Nevertheless, the impacts of this system operated jointly with other circulation features rather than functioning as the sole driver.

Further support comes from coupled climate model simulations. Daily outputs from the ACCESS-ESM1-5 historical experiment reproduce many of the key TPVSL features seen in reanalysis. In particular, the model captures both the spatiotemporal propagation of successive vortices in July and their horizontal structure, which closely resemble the observational fields (Fig. 1 vs. Fig. 4). Importantly, the cyclonic members of the simulated TPVSL extend far enough eastward to influence the Beijing region, underscoring the potential role of TPVSL activity in shaping rainfall variability over northern China. These examples are represen-

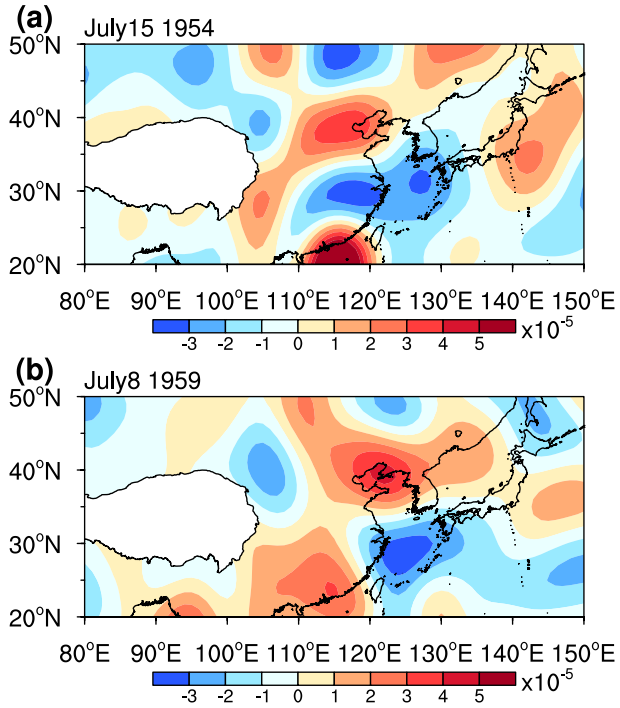

Fig. 4. Spatiotemporal structure of the TPVSL in historical simulations by ACCESS-ESM1-5. (a, b) Daily 700-hPa relative vorticity fields after low-pass spatial filtering on (a) 15 July 1954 and (b) 8 July 1959 (shading; units: 10^{-5} s^{-1}). These examples illustrate the model's ability to reproduce TPVSL structures, with alternating cyclonic and anticyclonic patterns consistent with reanalysis-based diagnostics. We note that these are representative cases selected from the full 1950–2014 ACCESS-ESM1-5 historical simulation, in which multiple TPVSL occurrences were identified.

tative of multiple TPVSL occurrences identified in the full historical simulation.

3.3. *Anomalous characteristics of the TPVSL in July 2025 and its linkage to the WPSH*

We further assessed key dynamical properties of the TPVSL during July 2025, including vortex translation speed, shedding period, intensity, and the meridional position of its propagation axis (Fig. 5). The mean propagation speed of vortices was 5.6 m s^{-1}, slightly higher than the climatological mean, while the shedding period averaged 4.5 days, slightly lower than normal. The mean intensity of the TPVSL, expressed as positive filtered vorticity, was 4.4 × 10^{-6} s^{-1}, also slightly weaker than the climatology. In contrast, the latitude of the propagation line reached ~39°N, substantially farther north than the climatological mean. This poleward displacement aligned the TPVSL activity with the Beijing region, positioning successive vortices directly over the local rain belt and sustaining the extreme rainfall. The spatial pattern of the TPVSL field in July 2025 (Figs. 6a, b) further confirms this anomalous northward displacement.

The anomalous northward displacement of the TPVSL propagation line appears to be closely associated with variability in the western Pacific subtropical high (WPSH). The latitude of the WPSH has long been recognized as a key regulator of the East Asian rain belt (Tao and Chen, 1987; Chiang et al., 2020). In addition, recent work has demonstrated that the propagation tracks of TPVSL vortex pairs tend to align with the northern margins of the WPSH (Liu et al., 2023). Our correlation analysis across different longitudes (Figs. 6c, d) further supports this connection: west of 135°E, the latitudinal positions of the TPVSL and the WPSH northern boundary exhibit strong correlations that are significant at the 95% confidence level; whereas east of 135°E, the correlation weakens and becomes statistically insignificant. Such a downstream-constrained relationship is consistent with the principles of vortex street dynamics where, once established, the propagation pathway of the vortices is largely dictated by the prevailing downstream flow. During boreal summer, this guiding flow is supplied by the northern flank of the WPSH, which anchors the TPVSL's northward shift and ties it to the position of the regional rain belt (Liu et al., 2023, 2025).

3.4. *The impacts of moisture content and atmospheric instability on this event*

Considering that this extreme rainfall event resulted from interactions among multiple factors, we also analyzed contributions from moisture transport not directly linked to

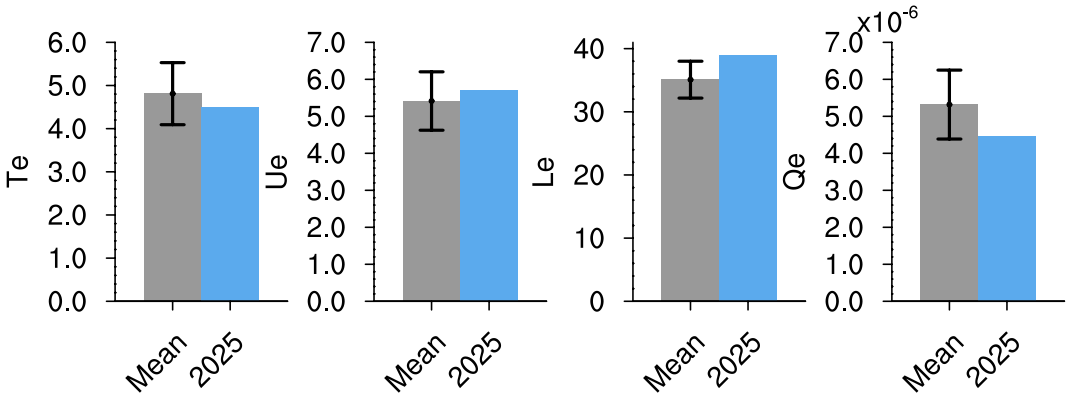

Fig. 5. Anomalous characteristics of TPVSL properties in July 2025. Distributions of climatological July means (grey) and July 2025 values (blue) for four key diagnostics of the TPVSL: shedding period (Te, days); vortex propagation speed (Ue, m s^{-1}); latitudinal position of the propagation line (Le, °N); and average intensity (Qe, s^{-1}).

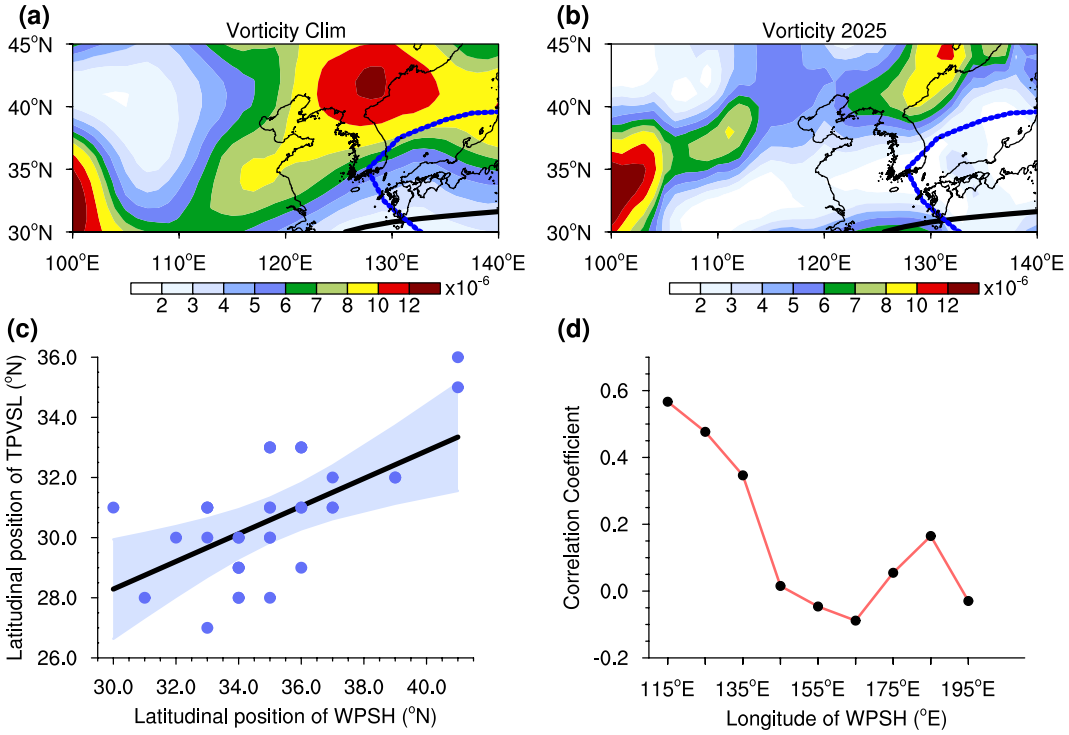

Fig. 6. Anomalous features of the TPVSL and its relationship with the Western Pacific Subtropical High (WPSH). (a) Climatological July mean (1981–2010) anomalies of the TPVSL (shading; units: s^{-1}), in which the position of the WPSH is indicated by blue and black contours, respectively. (b) As in (a) but for July 2025. (c) Scatterplot showing the relationship between the latitudinal position of the TPVSL propagation line and that of the northern edge of the WPSH (110°–130°E) during 1979–2024. (d) Correlation coefficients (red) between the TPVSL propagation latitude and the WPSH northern boundary across longitudes.

TPVSL dynamics and atmospheric instability. Figure 7a shows the 850-hPa moisture flux and the magnitude of the vertically integrated moisture flux from the surface to 300 hPa on 24 July 2025. The results reveal two major moisture transport pathways: (1) the South China Sea pathway, where strong southwesterly flows transported abundant moisture from the South China Sea northward into North China; and (2) moisture transport along the periphery of the subtropical high influenced by the outer circulation of Typhoons Francisco and Co-may. These transport channels collectively formed a stable and efficient moisture conveyor belt over North China, providing sufficient moisture conditions for the extreme rainfall event in Beijing. Figure 7b presents the spatial distribution of CAPE in the Beijing area from 24 to 28 July. It can be seen that Beijing was located in a region of high CAPE values. Favorable energy conditions were present throughout the event, with a notable increase in CAPE starting from 0800 UTC 24 July, providing strong atmospheric instability conducive to the extreme rainfall in Beijing.

3.5. *Sensitivity experiment by removing the TPVSL*

We first arranged the initial conditions for the CTRL and NO_TPVSL experiments. It is evident that the vortex street band extending eastward from the Tibetan Plateau has been significantly flattened. Only large-scale background structures remain in the Beijing area. The model simulation results based on the original fields are shown in Fig. 8. The results indicate that both the CTRL and NO_TPVSL fields exhibit a large precipitation center in the Beijing area. The spatial distribution pattern of precipitation in the model and the magnitude of the precipitation peak are roughly consistent with the observations of this heavy rainfall event in Beijing. This suggests that this idealized experiment has a good simulation capability for this extreme precipitation event. However, the NO_TPVSL field almost entirely lacks precipitation exceeding 150 mm d^{-1}, whereas grid points exceeding 150 mm d^{-1} are very prominent in the CTRL field over the Beijing region. This indicates that weakening the TPVSL field has a strong dampening effect on this extreme precipitation event, supporting the notion that the TPVSL provides a favorable background for precipitation.

3.6. *Strengthened northward displacement of the WPSH and TPVSL increases the likelihood of Beijing-type extreme rainfall*

The anomalous northward and westward displacement of the WPSH and the primary rain belt during July 2025 reflected both interannual variability and a long-term trend. At the interannual scale, the persistent northward migration of two TCs contributed to sustaining the poleward shift of the WPSH and its associated rain belt, a mechanism well documented in previous studies (Wu, 1999; Huang et al., 2016). Here, however, we focus on the contribution of the long-

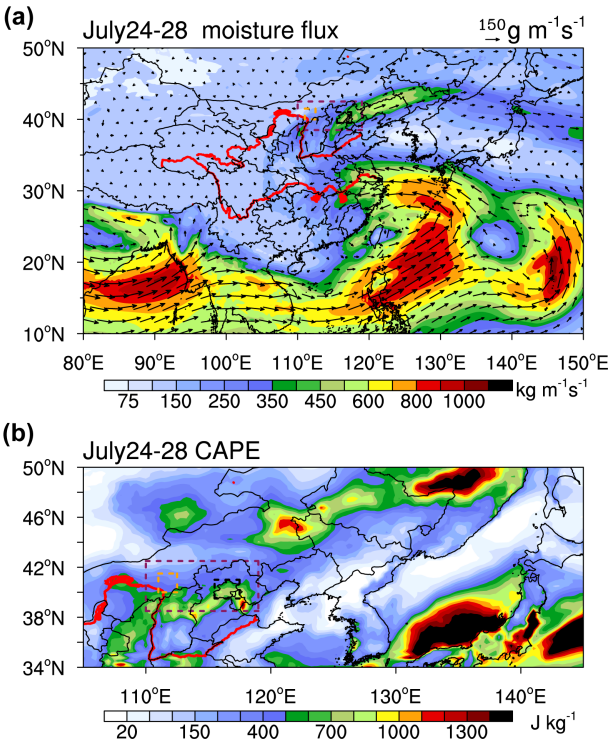

Fig. 7. (a) The 850-hPa moisture flux (vectors; units: 150 g m^{-1} s^{-1}) and the magnitude of the vertically integrated moisture flux from the surface to 300 hPa (shaded; units: kg m^{-1} s^{-1}) on 24 July 2025. (b) Spatial distribution of the mean convective available potential energy (CAPE) in the Beijing area from 24 to 28 July.

term displacement of the summer rain belt.

Figures 9a–c show the spatiotemporal evolution of summer precipitation across eastern China from 1979 to 2024, along with its monthly components. Most regions experienced positive anomalies in seasonal mean precipitation, except for portions of central China, which displayed slight decreases. Enhanced precipitation in June was concentrated in southern China, whereas in July–August the increase was strongest over North China, particularly around Beijing, with rates of 0.06–0.08 mm d^{-1} yr^{-1}, significant at the 95% confidence level. This pattern was primarily driven by enhanced precipitation associated with TPVSL activity (Figs. 9d–f). The intensification of heavy rainfall exceeding 50 mm d^{-1} closely mirrored the pattern of total precipitation change (Figs. 9g–i), indicating that the observed July–August increase in both mean rainfall and extremes around Beijing was mainly attributable to cyclonic vortices embedded within the TPVSL.

The spatial structure of this precipitation increase is consistent with the dynamics of the TPVSL and its linkage to the WPSH. Figure 10a depicts the climatological mean and anomalies in the TPVSL's summer evolution. The system tends to be displaced southward in June but shifts anomalously northward in July and August. Notably, the poleward migration of the WPSH has accelerated in recent decades. Along 120°–130°E, the WPSH axis advanced northward by 7° intraseasonally between 1979 and 2001 (from 24°N in June to 31°N in August). Between 2002 and 2024, this

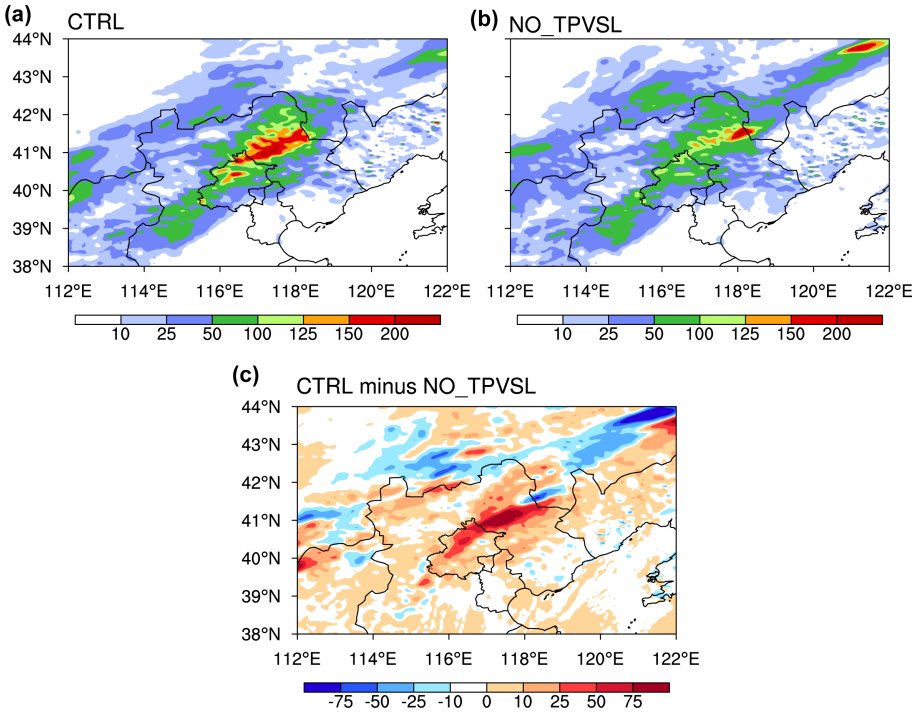

Fig. 8. The 24-hour accumulated precipitation (units: mm) from 0000 UTC 24 July to 0000 UTC 25 July 2025: a comparison between the CTRL and NO_TPVSL experiments. (a) Simulated precipitation in the CTRL experiment. (b) Simulated precipitation in the NO_TPVSL experiment, in which the TPVSL has been removed. (c) Difference between the two experiments (CTRL minus NO_TPVSL).

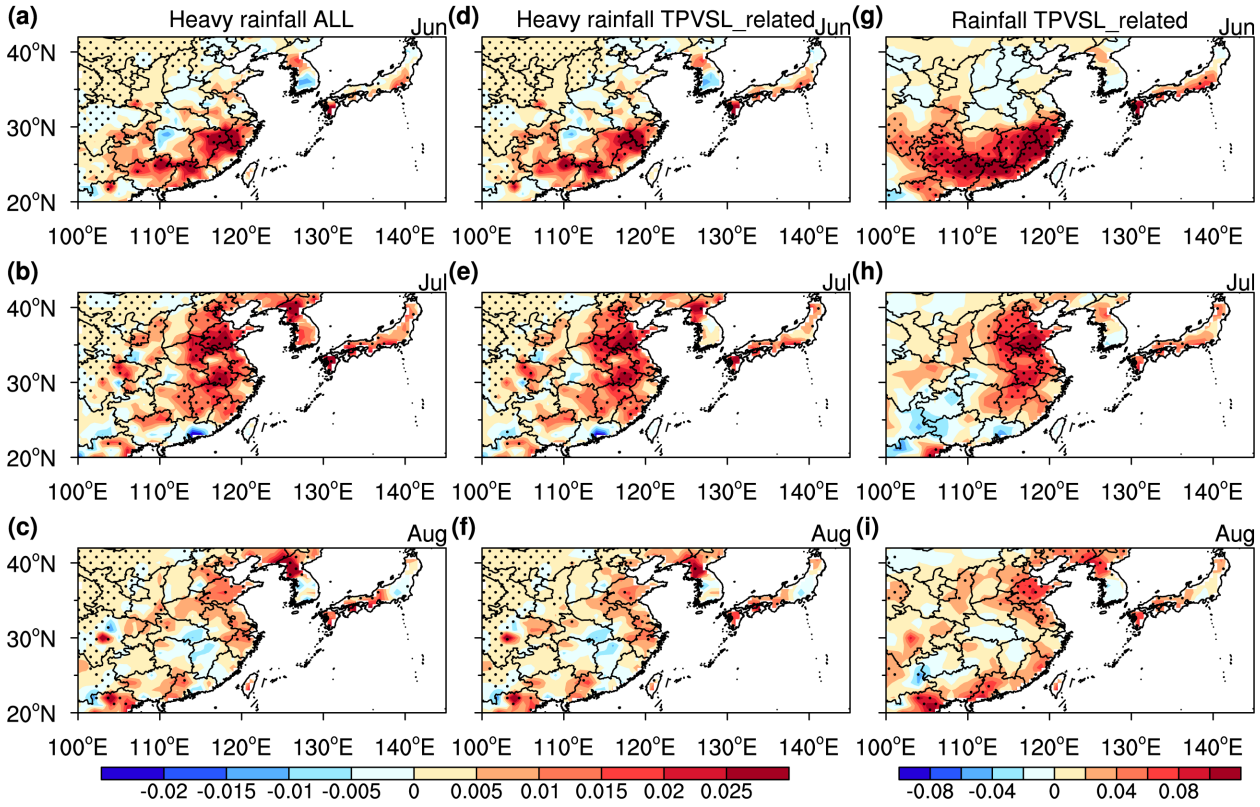

Fig. 9. Long-term trends in heavy rainfall and TPVSL-related precipitation. (a–c) Secular trends in the number of heavy rainfall days (daily precipitation ⩾ 50 mm; units: d yr^{-1}) during (a) June, (b) July, and (c) August for the period 1979–2024. (d–f) As in (a–c) but for TPVSL-related heavy rainfall days (units: d yr^{-1}). (g–i) As in (a–c) but for TPVSL-related daily precipitation (units: mm d^{-1} yr^{-1}).

advance reached 9° (from 23°N in June to 32°N in August). Such behavior is consistent with vortex-street dynamics, in which the propagation of vortices is guided by the background flow, with the northwestern flank of the WPSH serving as the key pathway in boreal summer.

In addition, long-term diagnostics (Fig. 10b) confirm that both the WPSH and the TPVSL have undergone a statistically significant poleward displacement over the past five decades. These findings imply that the accelerated intraseasonal northward migration of the TPVSL and the WPSH during July–August has increased the likelihood of extreme rainfall in North China, thereby raising the probability of Beijing-type flood-producing events.

4. Discussion and conclusions

Using daily reanalysis data and precipitation observations, we quantified the contribution of the TPVSL system to the late-July 2025 heavy rainfall over the Beijing region. Our analysis shows that this system provided an important circulation background; specifically, providing a favorable background for nearly 90% of the observed precipitation. The WRF-based sensitivity experiments showed that, after removing the TPVSL, precipitation in the Beijing area decreased significantly, supporting the notion that the TPVSL provided a favorable background for precipitation. Based on the vorticity budget analysis, horizontal advection provided a sustained positive contribution before and during the rainfall peak, while the stretching term became increasingly important during the peak period, which is consistent with a previous study (Fu et al., 2022a).

The TPVSL during this episode exhibited an exceptionally northward-displaced propagation line, while its shedding period, propagation speed, and intensity remained close to their climatological means. This anomalous displacement shifted the primary summer rain belt into northern China, thereby creating favorable conditions for prolonged and extreme rainfall around Beijing.

As suggested by previous studies, the summer propagation of the TPVSL is guided by the northwestern flank of the WPSH. The unusual poleward anomaly in July 2025 arose from the concurrent northward displacement of the WPSH, amplified by the tracks of two typhoons. Beyond this single event, both the WPSH and the TPVSL pathway have displayed a systematic northward trend over the past five decades in July–August, implying a growing likelihood of TPVSL-related extreme rainfall events in northern China. Such a trend may be linked to the poleward expansion of the Hadley circulation and other large-scale circulation changes.

While our findings establish the TPVSL as a favorable background system for the July 2025 Beijing floods, the

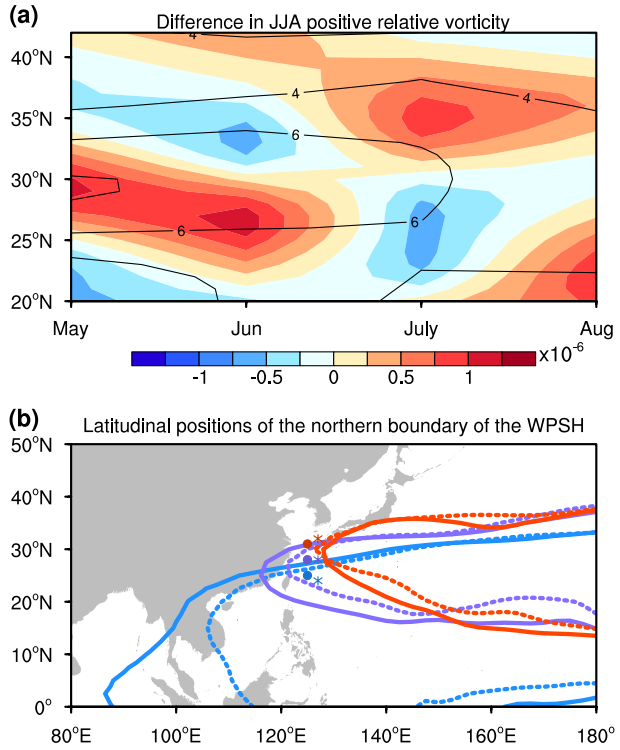

Fig. 10. Long-term changes in the spatiotemporal structure of the TPVSL and its link to the WPSH. (a) Difference in the June–August anomaly of positive relative vorticity at 700 hPa between 2002–24 and 1979–2001 (shading; units: 10^{-6} s^{-1}). Values are averaged over 110°–120°E. The 1981–2020 climatological mean of positive vorticity is overlaid as black contours (interval: 10^{-6} s^{-1}). (b) Latitudinal positions of the northern boundary of the WPSH for June (blue), July (purple), and August (red), shown for the two periods 1979–2001 (dotted lines) and 2002–24 (solid lines). The markers indicate the mean latitudinal position averaged over 120°–130°E (dots: 1979–2001; stars: 2002–24).

event was not determined by this factor alone. Instead, it resulted from multiscale interactions. For example, the transport channels of the moisture conveyor belt over North China and the large center of CAPE also provide favorable conditions for the extreme rainfall event in Beijing. By situating this extreme rainfall within the dynamics of the TPVSL, our study provides a new perspective on the mechanisms shaping northern China's hydroclimate and highlights the need to incorporate vortex street dynamics into future flood risk assessment and disaster mitigation strategies.

It is important to note that the present analysis deliberately focuses on the role of the TPVSL in shaping the large-scale circulation background of the July 2025 Beijing extreme rainfall. Other dynamical and thermodynamical factors, including moisture transport pathways, convective instability, and local mesoscale processes, also contributed to the event, and a more comprehensive assessment integrating these processes remains an important topic for future investigation.

In terms of future changes, fluid dynamics considerations suggest that the northern boundary of the WPSH provides the basic flow direction for the eastward propagation of the TPVSL. As the WPSH is projected to extend westward and shift northward under future climate scenarios, a further northward displacement of the TPVSL and an increased likelihood of TPVSL-related summer heavy rainfall over Beijing may be expected. However, substantial interdecadal variability of the WPSH (Huang et al., 2016), which is projected to intensify under global warming (Yang et al., 2022), adds uncertainty to such projections.

Acknowledgements. This work was supported by the National Natural Science Foundation of China (Grant No. 42406006).

Data Availability Statement The NCEP–NCAR reanalysis dataset is available at https://esrl.noaa.gov/psd/data/gridded/data.ncep.reanalysis.html. The CPC precipitation dataset is available at https://psl.noaa.gov/data/gridded/data.cpc.globalprecip.html. The ERA5 dataset is available from the Copernicus Climate Data Store at https://cds.climate.copernicus.eu/datasets.

REFERENCES

Bearman, P. W., 1967: On vortex street wakes. *J. Fluid Mech.*, **28**, 625–641, https://doi.org/10.1017/S0022112067002368.

Chen, F., and J. Dudhia, 2001: Coupling an advanced land surface–hydrology model with the Penn State–NCAR MM5 modeling system. Part I: Model implementation and sensitivity. *Mon. Wea. Rev.*, **129**, 569–585, https://doi.org/10.1175/1520-0493(2001)129<0569:CAALSH>2.0.CO;2.

Chen, M. Y., W. Shi, P. P. Xie, V. B. S. Silva, V. E. Kousky, R. Wayne Higgins, and J. E. Janowiak, 2008: Assessing objective techniques for gauge-based analyses of global daily precipitation. *J. Geophys. Res.*, **113**, D04110, https://doi.org/10.1029/2007JD009132.

Chen, Y. R., and Coauthors, 2023: Relative contribution of moisture transport during TC-active and TC-inactive periods to the precipitation in Henan Province of North China: Mean state and an extreme event. *J. Climate*, **36**, 3611–3623, https://doi.org/10.1175/JCLI-D-22-0582.1.

Chen, Z. H., and J. Zhang, 2020: The characteristics of late summer extreme precipitation in northern China and associated large‐scale circulations. *International Journal of Climatology*, **40**, 5170–5187, https://doi.org/10.1002/joc.6512.

Chiang, J. C. H., W. Kong, C. H. Wu, and D. S. Battisti, 2020: Origins of East Asian summer monsoon seasonality. *J. Climate*, **33**, 7945–7965, https://doi.org/10.1175/JCLI-D-19-0888.1.

Chopra, K. P., and L. F. Hubert, 1965: Mesoscale eddies in wake of islands. *J. Atmos. Sci.*, **22**, 652–657, https://doi.org/10.1175/1520-0469(1965)022<0652:MEIWOI>2.0.CO;2.

Curio, J., R. Schiemannm, K. I. Hodges, and A. G. Turner, 2019: Climatology of Tibetan Plateau vortices in reanalysis data and a high-resolution global climate model. *J. Climate*, **32**, 1933–1950, https://doi.org/10.1175/JCLI-D-18-0021.1.

Davis, C. A., and S. Low-Nam, 2001: The NCAR-AFWA Tropical Cyclone Bogussing Scheme. Air Force Weather Agency (AFWA) Rep, 12 pp.

Ding, Y. H., 1992: Effects of the Qinghai-Xizang (Tibetan) plateau on the circulation features over the plateau and its surrounding areas. *Adv. Atmos. Sci.*, **9**, 112–130, https://doi.org/

10.1007/BF02656935.

Ding, Y. H., 2015: On the study of the unprecedented heavy rainfall in Henan Province during 4-8 August 1975: Review and assessment. *Acta Meteor. Sinica*, **73**, 411–424, (in Chinese with English abstract) https://doi.org/10.11676/qxxb2015.067.

Ding, Y. H., and J. C. L. Chan, 2005: The East Asian summer monsoon: An overview. *Meteorol. Atmos. Phys.*, **89**, 117–142, https://doi.org/10.1007/s00703-005-0125-z.

Fu, S.-M., J.-H. Sun, Y.-L. Luo, and Y.-C. Zhang, 2017: Formation of long-lived summertime mesoscale vortices over central east China: Semi-idealized simulations based on a 14-year vortex statistic. *J. Atmos. Sci.*, **74**, 3955–3979, https://doi.org/10.1175/JAS-D-16-0328.1.

Fu, S.-M., H. Tang, J.-H. Sun, T.-B. Zhao, and W.-L. Li, 2022a: Historical rankings and vortices' activities of the extreme Mei-yu seasons: Contrast 2020 to previous Mei-yu seasons. *Geophys. Res. Lett.*, **49**, e2021GL096590, https://doi.org/10.1029/2021GL096590.

Fu, S.-M., Y.-C. Zhang, H.-J. Wang, H. Tang, W.-L. Li, and J.-H. Sun, 2022b: On the evolution of a long-lived mesoscale convective vortex that acted as a crucial condition for the extremely strong hourly precipitation in Zhengzhou. *J. Geophys. Res.*, **127**, e2021JD036233, https://doi.org/10.1029/2021JD036233.

Fu, S.-M., J.-P. Zhang, X. Xiao, T.-T. Huang, and J.-H. Sun, 2025: A 42-Year statistic on the dabie vortices: Multiscale temporal characteristics and associated mechanisms, and hourly rainfall features. *J. Climate*, **38**, 1553–1572, https://doi.org/10.1175/JCLI-D-24-0304.1.

Hanley, J., and R. Caballero, 2012: Objective identification and tracking of multicentre cyclones in the ERA‐Interim reanalysis dataset. *Quart. J. Roy. Meteor. Soc.*, **138**, 612–625, https://doi.org/10.1002/qj.948.

Hersbach, H., and Coauthors, 2020: The ERA5 global reanalysis. *Quart. J. Roy. Meteor. Soc.*, **146**(730), 1999–2049, https://doi.org/10.1002/qj.3803.

Holton, J. R., 1992: *An Introduction to Dynamic Meteorology*. 3rd ed., Academic Press, 1–497.

Hong, S.-Y., and J.-O. J. Lim, 2006: The WRF single-moment 6-class microphysics scheme (WSM6). *Journal of the Korean Meteorological Society*, **42**, 129–151.

Hong, S.-Y., Y. Noh, and J. Dudhia, 2006: A new vertical diffusion package with an explicit treatment of entrainment processes. *Mon. Wea. Rev.*, **134**, 2318–2341, https://doi.org/10.1175/MWR3199.1.

Huang, R. H., and Y. F. Wu, 1989: The influence of ENSO on the summer climate change in China and its mechanism. *Adv. Atmos. Sci.*, **6**, 21–32, https://doi.org/10.1007/BF02656915.

Huang, Y. Y., X. F. Li, and H. J. Wang, 2016: Will the western Pacific subtropical high constantly intensify in the future? *Climate Dyn.*, **47**(1), 567–577, https://doi.org/10.1007/s00382-015-2856-y.

Iacono, M. J., J. S. Delamere, E. J. Mlawer, M. W. Shephard, S. A. Clough, and W. D. Collins, 2008: Radiative forcing by long‐lived greenhouse gases: Calculations with the AER radiative transfer models. *J. Geophys. Res.*, **113**, D13103, https://doi.org/10.1029/2008JD009944.

Kain, J. S., 2004: The Kain–Fritsch convective parameterization: An update. *J. Appl. Meteorol.*, **43**, 170–181, https://doi.org/10.1175/1520-0450(2004)043<0170:TKCPAU>2.0.CO;2.

Kalnay, E., and Coauthors, 1996: The NCEP/NCAR 40-year reanalysis project. *Bull. Amer. Meteor. Soc.*, **77**, 437–472, https://doi.org/10.1175/1520-0477(1996)077<0437:TNYRP>2.0.CO;2.

Khan, N. B., Z. Ibrahim, L. T. T. Nguyen, M. F. Javed, and M. Jameel, 2017: Numerical investigation of the vortex-induced vibration of an elastically mounted circular cylinder at high Reynolds number (Re=10^4) and low mass ratio using the RANS code. *PLoS One*, **12**(10), e0185832, https://doi.org/10.1371/journal.pone.0185832.

Kirk, J. R., 2003: Comparing the dynamical development of two mesoscale convective vortices. *Mon. Wea. Rev.*, **131**, 862–890, https://doi.org/10.1175/1520-0493(2003)131<0862:CTDDOT>2.0.CO;2.

Kong, W. W., and J. C. H. Chiang, 2020: Interaction of the westerlies with the Tibetan Plateau in determining the mei-yu termination. *J. Climate*, **33**, 339–363, https://doi.org/10.1175/JCLI-D-19-0319.1.

Li, L., C. W. Zhu, R. H. Zhang, and B. Q. Liu, 2021: Roles of the Tibetan Plateau vortices in the record Meiyu rainfall in 2020. *Atmos. Sci. Lett.*, **22**, e1017, https://doi.org/10.1002/asl.1017.

Liu, H. B., D.-L. Zhang, and B. Wang, 2008: Daily to submonthly weather and climate characteristics of the summer 1998 extreme rainfall over the Yangtze River Basin. *J. Geophys. Res.*, **113**, D22101, https://doi.org/10.1029/2008JD010072.

Liu, Q., C. B. Fu, and Z. F. Xu, 2025: The key role of abnormal Vortex Street-like system in the Tibetan Plateau's wake in modulating extreme June-July rainfall events over Eastern China (2020 and 2024). *Climate Dyn.*, **63**, 216, https://doi.org/10.1007/s00382-025-07708-6.

Liu, Q., Z. H. Wu, Z.-M. Tan, F. C. Yang, and C. B. Fu, 2023: The atmospheric vortex streets and their impact on precipitation in the wake of the Tibetan Plateau. *Atmosphere*, **14**, 1096, https://doi.org/10.3390/atmos14071096.

Luo, Y. L., M. W. Wu, F. M. Ren, J. Li, and W.-K. Wong, 2016: Synoptic situations of extreme hourly precipitation over China. *J. Climate*, **29**, 8703–8719, https://doi.org/10.1175/JCLI-D-16-0057.1.

Luo, Y. L., J. H. Zhang, M. Yu, X. D. Liang, R. D. Xia, Y. Y. Gao, X. Y. Gao, and J. F. Yin, 2023: On the influences of urbanization on the extreme rainfall over Zhengzhou on 20 July 2021: A convection-permitting ensemble modeling study. *Adv. Atmos. Sci.*, **40**, 393–409, https://doi.org/10.1007/s00376-022-2048-8.

O'Neill, B. C., and Coauthors, 2016: The scenario model intercomparison project (ScenarioMIP) for CMIP6. *Geoscientific Model Development*, **9**, 3461–3482, https://doi.org/10.5194/gmd-9-3461-2016.

Orsolini, Y. J., L. Zhang, D. H. W. Peters, K. Fraedrich, X. H. Zhu, A. Schneidereit, and B. van den Hurk, 2015: Extreme precipitation events over north China in August 2010 and their link to eastward‐propagating wave‐trains across Eurasia: Observations and monthly forecasting. *Quart. J. Roy. Meteor. Soc.*, **141**, 3097–3105, https://doi.org/10.1002/qj.2594.

Sun, W., J. Li, R. C. Yu, and W. H. Yuan, 2015: Two major circulation structures leading to heavy summer rainfall over central North China. *J. Geophys. Res.*, **120**, 4466–4482, https://doi.org/10.1002/2014JD022853.

Tao, S.-Y., and Y.-H. Ding, 1981: Observational evidence of the influence of the Qinghai-Xizang (Tibet) Plateau on the occur-

rence of heavy rain and severe convective storms in China. *Bull. Amer. Meteor. Soc.*, **62**, 23–30, https://doi.org/10.1175/1520-0477(1981)062<0023:OEOTIO>2.0.CO;2.

Tao, S. Y., and L. X. Chen, 1987: A review of recent research on the East Asian summer monsoon in China. *Monsoon Meteorology*, C.-P. Chang, and T. N. Krishnamurti, Eds., Oxford University Press, 60–92.

Wang, X. M., and Y. Liu, 2017: Causes of extreme rainfall in May 2013 over Henan Province: The role of the southwest vortex and low-level jet. *Theor. Appl. Climatol.*, **129**, 701–709, https://doi.org/10.1007/s00704-017-2054-4.

Wheeler, M., and G. N. Kiladis, 1999: Convectively coupled equatorial waves: Analysis of clouds and temperature in the wavenumber–frequency domain. *J. Atmos. Sci.*, **56**, 374–399, https://doi.org/10.1175/1520-0469(1999)056<0374:CCEWAO>2.0.CO;2.

Wu, R. S., 1999: *Principles of Modern Synoptic Meteorology*. Higher Education Press.

Xu, J., R. M. Li, Q. H. Zhang, Y. Chen, X. D. Liang, and X. J. Gu, 2022: Extreme large-scale atmospheric circulation associated with the "21·7" Henan flood. *Science China Earth Sciences*, **65**, 1847–1860, https://doi.org/10.1007/s11430-022-9975-0.

Yang, K., W. J. Cai, G. Huang, K. M. Hu, B. Ng, and G. J. Wang, 2022: Increased variability of the western Pacific subtropical high under greenhouse warming. *Proceedings of the National Academy of Sciences of the United States of America*, **119**(23): e2120335119, https://doi.org/10.1073/pnas.2120335119.

Yeh, T.-C., and Y. X. Gao, 1979: *Tibet Plateau Meteorology*. Science Press, Beijing.

Zhang, D.-L., Y. H. Lin, P. Zhao, X. D. Yu, S. Q. Wang, H. W. Kang, and Y. H. Ding, 2013: The Beijing extreme rainfall of 21 July 2012: "Right results" but for wrong reasons. *Geophys. Res. Lett.*, **40**, 1426–1431, https://doi.org/10.1002/grl.50304.

Zhang, Q. H., R. M. Li, J. Z. Sun, F. Lu, J. Xu, and F. Zhang, 2023: A review of research on the record-breaking precipitation event in Henan Province, China, July 2021. *Adv. Atmos. Sci.*, **40**, 1485–1500, https://doi.org/10.1007/s00376-023-2360-y.

Zhao, Y., X. D. Xu, T. L. Zhao, and X. J. Yang, 2019a: Effects of the Tibetan Plateau and its second staircase terrain on rainstorms over North China: From the perspective of water vapour transport. *International Journal of Climatology*, **39**, 3121–3133, https://doi.org/10.1002/joc.6000.

Zhao, Y., and Coauthors, 2019b: The large‐scale circulation patterns responsible for extreme precipitation over the North China plain in midsummer. *J. Geophys. Res.*, **124**, 12 794–12 809, https://doi.org/10.1029/2019JD030583.

Zhou, T. J., F. F. Song, R. P. Lin, and X. Y. Chen, 2013: The 2012 North China floods: Explaining an extreme rainfall event in the context of a longer-term drying tendency. *Bull. Amer. Meteor. Soc.*, **94**, S49–S51.